Supporting Information for

# Reactivity of hydride bridges in a high-spin $[Fe_3(\mu\text{-}H)_3]^{3+}$ cluster: reversible $H_2$/CO exchange and Fe–H/B–F bond metathesis

Kevin J. Anderton[a], Brian J. Knight[a], Arnold L. Rheingold[c], Khalil A. Abboud[b], Ricardo García-Serres[d] and Leslie J. Murray[a,]*

[a] Center for Catalysis and [b]Department of Chemistry, University of Florida, Gainesville, Florida 32611, United States
[c] Department of Chemistry and Biochemistry, University of California, San Diego, La Jolla, California 92093, United States
[d] Univ. Grenoble Alpes, LCBM/PMB and CEA, IRTSV/CBM/PMB and CNRS, LCBM UMR 5249, PMB 38000 Grenoble, France

## Table of Contents


| | | |
|---|---|---|
| **Experimental details** | | S2 |
| **Figure S1** | $^1$H NMR Spectrum of $Fe_3H_3$**L** (**1**) | S5 |
| **Figure S2** | $^1$H NMR Spectrum of $Fe_3D_3$**L** (**1-D$_3$**) | S6 |
| **Figure S3** | $^1$H NMR spectrum of $(FeCO)_2Fe(\mu_3\text{-}H)$**L** (**2**) | S7 |
| **Figure S4** | $^1$H NMR Spectrum of $Fe_3F_3$**L** (**3**) | S8 |
| **Figure S5** | $^1$H NMR spectrum of attempted H/D exchange reaction between **1-D$_3$** and $H_2$ | S9 |
| **Figure S6** | Portion of the $^1$H NMR spectrum of the reaction of **1** with CO showing generation of $H_2$ | S10 |
| **Figure S7** | Portion of the $^1$H NMR spectrum of the reaction of a mixture of **1** and **1-D$_3$** with CO showing generation of $H_2$ but not HD | S11 |
| **Figure S8** | $^1$H NMR spectrum of the reaction of **2** with $H_2$ | S12 |
| **Figure S9** | $^{11}$B NMR spectrum of the reaction of **1** with $BF_3$•$OEt_2$ after addition of $NEt_3$ | S13 |
| **Figure S10** | IR spectrum of $(FeCO)_2Fe(\mu_3\text{-}H)$**L** (**2**) | S14 |
| **Figure S11** | IR spectrum of $Fe_3F_3$**L** (**3**) | S15 |
| **Figure S12** | IR spectrum of $(Fe\,^{13}CO)_2Fe(\mu_3\text{-}H)$**L** (**2-$^{13}$CO**) | S16 |
| **Figure S13** | Powder X-band EPR spectrum of **2** in parallel mode at 5 K | S17 |
| **Figure S14** | UV-vis spectrum of $(FeCO)_2Fe(\mu_3\text{-}H)$**L** (**2**) | S18 |
| **Figure S15** | UV-vis spectrum of $Fe_3F_3$**L** (**3**) | S19 |
| **Figure S16** | Plot of C-O distance versus Fe-C distance for **2** compared with complexes in the CSD featuring the monocarbonyliron motif | S20 |
| **Figure S17** | Plot of C-O distance versus Fe-C distance for **2** compared with iron carbonyl complexes in the CSD featuring Fe···CO semi-bridging interactions similar to those in **2** | S21 |
| **Figure S18** | Top-down view of the solid state structure of $(FeCO)_2Fe(\mu_3\text{-}H)$**L** (**2**) showing the minor occupied site for Fe1 | S22 |
| **Figure S19** | 4.8 K Mössbauer spectra of **2** measured in different parallel applied magnetic fields | S23 |
| **Table S1** | Simulation parameters for the Mössbauer spectrum of **2** measured under zero applied field at 80 K | S24 |
| **Table S2** | Selected bond distances and angles of $Fe_3H_3$**L** (**1**) and $Fe_3F_3$L (**3**) and comparison with other iron $\beta$-diketiminates | S25 |
| **Table S3** | Crystal data and structure refinement for **2** | S26 |
| **Table S4** | Crystal data and structure refinement for **3** | S27 |
| **References** | | S28 |

**General considerations.** Unless specified otherwise, all operations were performed under a dry, air-free atmosphere using an argon- or dinitrogen-filled MBraun Unilab glovebox or standard Schlenk techniques. $^1$H NMR spectra were recorded on a Varian Unity Inova 500 MHz spectrometer. Chemical shifts were referenced to solvent resonances at $\delta_H$ = 1.73 and 3.58 ppm for THF-$d_8$, at $\delta_H$ = 2.08, 6.97, 7.01, and 7.09 ppm for toluene-$d_8$, and at $\delta_H$ = 7.27 for $CDCl_3$. Protio impurities from the NMR solvent are marked with asterisks in the spectra. Solution magnetic susceptibilities were determined by the Evans method[1]. Infrared spectra were recorded in a nitrogen-filled glovebox as solids on a Bruker Alpha FTIR with an ATR diamond crystal stage using the Opus 7.0 software package or on a Cary 630 1B FTIR with an ATR diamond crystal using the Agilent Microlab software package. EPR samples were loaded in quartz tubes (4 x 5mm i.d. x o.d.) in an Ar-filled glovebox and sealed with gas-tight screw caps. EPR spectra were collected on a Bruker ELEXSYS E500 spectrometer fitted with a Bruker DM4116 dual-mode resonator, and temperature was maintained using an Oxford Instruments ESR900 continuous flow helium cryostat fitted with a Lakeshore Cryotronics Cernox sensor and monitored with a Lakeshore Model 336 Temperature Controller. Samples for UV/visible spectroscopy were prepared under an Ar atmosphere using air-free anhydrous THF, transferred to air-tight cuvettes (Starna Cells, Atascadero, CA, USA), and spectra recorded using an Agilent Cary 50 spectrophotometer. Mössbauer samples were ground, placed in Delrin sample containers, and sealed with screw caps in an Ar-filled glovebox. Mössbauer spectra were measured either on a low-field Mössbauer spectrometer equipped with a closed-cycle SHI-850-5 cryostat from Janis and SHI or an Oxford Instruments Spectromag 4000 cryostat containing an 8T split-pair superconducting magnet. Both spectrometers were operated in constant acceleration mode in transmission geometry. The isomer shifts are referenced against a room temperature metallic iron foil, and analysis of the data was performed using the program WMOSS (WEB research). Searches of the Cambridge Structure Database (CSD) were performed with Cambridge Crystallographic Data Center ConQuest software package using CSD version 5.37 Update 2 (Feb 2016). Significant outliers from the plots of the data generated were manually inspected and removed in cases of disorder. Tetrahydrofuran (THF), toluene, benzene, pentane, and dichloromethane were purified using either a Glass-Contour or Innovative Technologies solvent purification system and stored over 3 Å molecular sieves prior to use. The water content of each solvent was measured using a Mettler Toledo C20 Coulometric Karl Fischer Titrator prior to use and was below 1 ppm in all cases. Celite and 3 Å molecular sieves were dried at 220 °C under vacuum overnight. $Fe_3H_3$**L** (**1**)[2] and $LiBEt_3D$[3] were prepared according to previous reports. CO (UHP grade, 99.9%) and $H_2$ (UHP grade, 99.999%) were purchased from Airgas, Inc. and purified by passage through two cold traps ($LN_2$/*i*-PrOH). $^{13}$CO was purchased from Sigma-Aldrich and used as received. Deuterated solvents were purchased from Sigma-Aldrich or Cambridge Isotope Laboratories, dried using standard methods, and stored over 3 Å molecular sieves. All other reagents were purchased from Sigma-Aldrich and used without further purification.

**$^1$H NMR of $Fe_3H_3$L (1).** $\delta$ (toluene-$d_8$) = -44.67 (12H), -19.73 (18H), -6.92 (18H), -0.65 (3H), 79.77 (12H).

**$Fe_3D_3$L (1-D).** The synthesis followed the reported procedure for $Fe_3H_3$**L** (**1**)[2], but with $LiBEt_3D$ instead of $KBEt_3H$. $^1$H NMR (toluene-$d_8$): $\delta$ = -44.69 (12H), -19.50 (18H), -6.96 (18H), -0.53 (3H), 79.23 (12H). No characteristic Fe-D vibration was observed in the IR spectrum.

**$(FeCO)_2Fe(\mu_3$-H)L** (**2**). A 200 mL Schlenk flask was charged with $Fe_3H_3$**L** (466.0 mg, 0.543 mmol), a Teflon-coated stir bar, and THF (65 mL). The solution was degassed by the freeze-pump-thaw method, then exposed to a slow flow of CO for 5 minutes with stirring. The flask was closed and the reaction was stirred for 2 hours, with a color change from dark red-orange to very dark yellow-green occurring over the first 20 minutes. After this time the reaction was evaporated and the residue was dissolved in boiling THF (65 mL). Cooling the solution to -35 $^o$C yielded dark yellow-green crystals (342.3 mg, 0.375 mmol, 69 %) after 2 d. Integration of the $^1$H NMR signal of the crude reaction product relative to an internal naphthalene standard indicates that the product forms in quantitative spectroscopic yield, such that the recrystallization step can be omitted without substantially affecting the purity. X-ray quality crystals were obtained by slow evaporation of a saturated THF solution in the presence of benzene. $^1$H NMR (toluene-$d_8$): $\delta$ = -57.14 (6H), -54.82 (1H), -35.36 (2H), -29.92 (4H), -17.60 (12H), -14.01 (4H), -3.55 (12H), 3.96 (6H), 5.62 (4H), 59.98 (4H), 78.11 (4H), 161.81 (4H). IR (cm$^{-1}$): 1846 ($\nu$ CO), 1526, 1429, 1398, 1371, 1339, 1016. $\mu_{eff}$ (toluene-$d_8$, 298 K) = 5.6 $\mu_B$. Anal. Found (calcd) for $C_{47}H_{64}N_6O_2Fe_3$: C, 61.85 (61.86); H, 7.08 (7.07); N, 8.71 (9.21).

**$(Fe^{13}CO)_2Fe(\mu_3\text{-}H)L$ ($2\text{-}^{13}CO$).** The synthesis was the same as for **2** except a static atmosphere of $^{13}CO$ instead of a slow flow of $^{12}CO$ was used. IR ($cm^{-1}$): 1804 ($\nu$ $^{13}CO$). No resonances were visible in the $^{13}C$ NMR.

**$Fe_3F_3L$ (3).** A scintillation vial was charged with $Fe_3H_3$**L** (60.0 mg, 0.0699 mmol), a Teflon-coated stir bar, and toluene (17 mL), followed by $BF_3$•$OEt_2$ (9.06 µL, 0.0734 mmol). The vial was then sealed with a Teflon-lined cap and stirred at ambient temperature. The red suspension progressively converted to a bright yellow solution. After 1.5 h, the reaction was passed through a toluene-rinsed celite plug and the resulting solution was evaporated. The bright yellow residue was then dissolved in boiling benzene (4 mL). Cooling the solution to ambient temperature yielded a bright yellow powder (36.4 mg, 0.0399 mmol, 57% yield) after 2 d. Integration of the $^1H$ NMR signal of the crude reaction product relative to an internal naphthalene standard indicates that the product forms in quantitative spectroscopic yield, such that the recrystallization step can be omitted without substantially affecting the purity. X-ray quality crystals were obtained by slow evaporation of a saturated dichloromethane solution in the presence of pentane. $^1H$ NMR (toluene-$d_8$): $\delta$ = -55.60 (18H), -39.01 (12H), -21.76 (3H), -13.04 (18H), 149.46 (12H). $^{19}F$ NMR showed no resonances between 500 and -500 ppm. IR ($cm^{-1}$): 1518, 1429, 1393, 1373, 1326, 1018, 516 ($\nu$ Fe-F). $\mu_{eff}$ (toluene-$d_8$, 298 K) = 7.4 $\mu_B$. HRMS (ESI+) m/z calcd for $(M)^+$ $[C_{45}H_{63}N_6F_3Fe_3]^+$: 912.3115, found 912.3123. Anal. Found (calcd) for $C_{45}H_{63}N_6F_3Fe_3(CH_2Cl_2)_{0.5}(C_5H_{12})$: C, 59.69 (59.38); H, 7.60 (7.37); N, 8.38 (8.48).

**Reaction of $Fe_3D_3L$ ($1\text{-}D_3$) with $H_2$.** A J. Young NMR tube was charged with a solution of $Fe_3D_3$**L** (2.0 mg, 2.3 $\mu$mol) in toluene-$d_8$ (400 $\mu$L). The tube was degassed by the freeze-pump-thaw method, allowed to warm to r.t., then filled with $H_2$. The tube was then closed, inverted, shaken, and refilled with $H_2$ three times to ensure saturation. A $^1H$ NMR spectrum was recorded after heating the reaction at 80 $^oC$ for 20 h. No shift in the resonances due to the PIECS effect was observed, consistent with the absence of exchange with $H_2$.

**Detection of $H_2$ in the reaction of $Fe_3H_3L$ (1) with CO.** A J. Young NMR tube was charged with a solution of $Fe_3H_3$**L** (2.1 mg, 2.4 $\mu$mol) and naphthalene (2.0 mg, 16 $\mu$mol) in THF-$d_8$ (400 $\mu$L). The tube was degassed by the freeze-pump-thaw method, allowed to warm to r.t., then filled with CO. The tube was then closed, inverted, shaken, and refilled with CO three times to ensure saturation. During this process, a rapid color change to dark yellow-green occurred. A $^1H$ NMR spectrum was recorded after 25 min. $H_2$ and **2** were both observed in 76(6) % spectroscopic yield relative to the naphthalene standard. The non-quantitative yield results from the decomposition of the product under sub-atmospheric pressures, which cannot be avoided due to the difficulty of rapidly and completely saturating the solution with gas in a J. Young tube.

**Detection of $H_2$ in the reaction of $Fe_3H_3L$ (1) and $Fe_3H_3L$ (1-D) with CO.** A J. Young NMR tube was charged with a solution of $Fe_3H_3$**L** (1.6 mg, 1.9 $\mu$mol) and $Fe_3D_3$**L** (1.6 mg, 1.9 $\mu$mol) in THF-$d_8$ (400 $\mu$L). The tube was degassed by the freeze-pump-thaw method, allowed to warm to 0 °C., then filled with CO. The tube was then closed, inverted, shaken, and refilled with CO three times to ensure saturation. During this process, a rapid color change to dark yellow-green occurred. A $^1H$ NMR spectrum was recorded after 30 min at 0 °C. $H_2$, **2**, and **2-D** were observed, while HD was not detected.

**Reaction of $(FeCO)_2Fe(\mu_3\text{-}H)L$ (2) with $H_2$.** A Parr bomb was charged with **2** (15.0 mg, 16.4 $\mu$mol), a Teflon-coated stir bar, and toluene (10 mL) under an Ar environment and sealed. The inlet connection to the vessel was purged for 2 min with $H_2$ before pressurizing the vessel to 20 bar. The reaction was heated at 80 °C with stirring for 2 h to afford a red solution, then depressurized and evaporated under reduced pressure. A $^1H$ NMR spectrum was recorded; **1** was observed in 75±7% spectroscopic yield relative to a naphthalene standard.

**Detection of $BH_3$ in the reaction of $Fe_3H_3L$ (1) with $BF_3$•$OEt_2$.** A J. Young NMR tube was charged with a solution of $Fe_3H_3$**L** (2.1 mg, 2.45 $\mu$mol) in toluene (200 µL) and then a solution of $BF_3$•$OEt_2$ (200 $\mu$L, 12.9 mM in toluene, 2.57 $\mu$mol). The tube was closed, inverted, and shaken. The mixture changed from a dark red to a bright yellow within 10 minutes. The cap was removed after 1 h and the solution was rapidly charged with $Et_3N$ (4.29 $\mu$L, 30.8 $\mu$mol). The tube was closed, inverted, and shaken again. A $^{11}B$ NMR spectrum was recorded, and the only boron containing compounds observed in the mixture were $Et_3NBF_3$ and $Et_3NBH_3$.

**Synthesis of $Et_3NBF_3$ as an NMR internal standard.** To a stirring solution of triethylamine (204 mg, 2.02 mmol) in THF (2.0 mL) was added $BF_3$•$OEt_2$ (274 $\mu$L, 2.22 mmol). The resulting light amber suspension was stirred at 23 °C for 1 h. The mixture was then concentrated by rotary evaporation, washed with cold $Et_2O$ (2 x 1 mL, 0 °C), and the concentrated under reduced pressure to afford $Et_3NBF_3$ (191 mg, 57% yield) as an amber oil. $^1$H NMR ($CDCl_3$): $\delta$ = 3.25-3.16 (comp. m, 6H), 1.39-1.30 (comp. m, 9H). $^{13}$C NMR ($CDCl_3$): $\delta$ = 47.0, 8.8. $^{11}$B NMR (toluene-$d_8$): $\delta$ = 0.17 (q, $^1J_{B–F}$ = 17.8 Hz). $^{19}$F NMR ($CDCl_3$): $\delta$ = -151.5. IR (cm$^{-1}$): 1475, 1401, 1009, 762. LRMS (ESI+) *m/z* calc'd for $(M + H – BF_3)^+$ $[169.1 + H – BF_3]^+$: 102.1, 102.1 found.

**Synthesis of $Et_3NBH_3$ as an NMR internal standard.** To stirring triethylamine (222 mg, 2.20 mmol) was added a solution of $BH_3$•THF (2.42 mL, 1 M in THF, 2.42 mmol) at ambient temperature. The clear solution was stirred for 1 h and then filtered through an ether-rinsed celite plug and concentrated by rotary evaporation to afford $Et_3NBH_3$ (253 mg, >99% yield) as a colorless oil. $^1$H NMR ($CDCl_3$): $\delta$ = 2.78 (q, $J$ = 7.5 Hz, 6 H), 1.42 (q, $^1J_{B–H}$ = 158.0 Hz, 3H) 1.19 (t, $J$ = 7.5 Hz, 9H). $^{13}$C NMR ($CDCl_3$): $\delta$ = 52.5, 8.7. $^{11}$B NMR (toluene-$d_8$): $\delta$ = -12.58. IR (cm$^{-1}$): 2381, 2326, 1163, 767. LRMS (ESI+) *m/z* calc'd for $(M + H – BH_3)^+$ $[115.1 + H – BH_3]^+$: 102.1, 102.1 found.

## X-ray crystallography.

$(FeCO)_2Fe(\mu_3\text{-}H)$**L** (**2**). X-Ray Intensity data were collected at 100 K on a Bruker **DUO** diffractometer using MoKα radiation ($\lambda$ = 0.71073 Å) and an APEXII CCD area detector.

Raw data frames were read by program SAINT[4] and integrated using 3D profiling algorithms. The resulting data were reduced to produce hkl reflections and their intensities and estimated standard deviations. The data were corrected for Lorentz and polarization effects and numerical absorption corrections were applied based on indexed and measured faces.

The structure was solved and refined in *SHELXTL2014*[5], using full-matrix least-squares refinement. The non-H atoms were refined with anisotropic thermal parameters and all of the H atoms were calculated in idealized positions and refined riding on their parent atoms. The asymmetric unit consists of the Fe3 complex, one benzene molecule in general position and two half benzene molecules (with each located on an inversion center). Thus, the ratio of complex-to-solvent is 1-to-2. In the core of the complex, there are three Fe centers with one of them, Fe1 disordered over three positions and is refined in these three positions namely Fe1, Fe1' and Fe1". Fe1' and Fe1" are present only in trace amounts. Their site occupation factors, refined in the early stages of refinement, were fixed at 3.5% and 2.5% for Fe1' and Fe1", respectively. The three Fe centers are connected by two CO ligands and a hydride ligand. The hydride refined with negative displacement parameter indicating that there is more than 1 electron density in the position. The proton, H1, which is refined at 96% occupancy, is sharing the same position with traces of a hydroxyl oxygen, O1, of 4%. The proton of the 4% O1 hydroxyl ligand was not included in the final refinement model. Ligands H1/O1 link the Fe2 and Fe3 centers while the Fe1 is linked to Fe2 by C2'-O2, and to Fe3 by C3'-O3. There are no other disorders in the structure. In the final cycle of refinement, 12038 reflections (of which 9908 are observed with $I > 2\sigma(I)$) were used to refine 655 parameters and the resulting $R_1$, $wR_2$ and S (goodness of fit) were 3.04%, 8.20% and 1.085, respectively. The refinement was carried out by minimizing the $wR_2$ function using $F^2$ rather than F values. $R_1$ is calculated to provide a reference to the conventional R value but its function is not minimized.

$Fe_3F_3$**L** (**3**). A brown crystal was mounted on a Cryo-Loop with Paratone-N. Data were collected on a Bruker Ultra diffractometer equipped with a rotating-anode source and micro-focus optics at 100K. All aspects of the data collection and subsequent processing of the data employed standard practices using software contained in the ApexIII and Olex2 libraries of programs. The diffuse contributions of unidentified solvent totaling 108e$^-$/unit cell in four equal voids were removed using the SQUEEZE routine in the Platon library of programs. ADDSYM, also part of the Platon library, confirmed that space-group assignment.

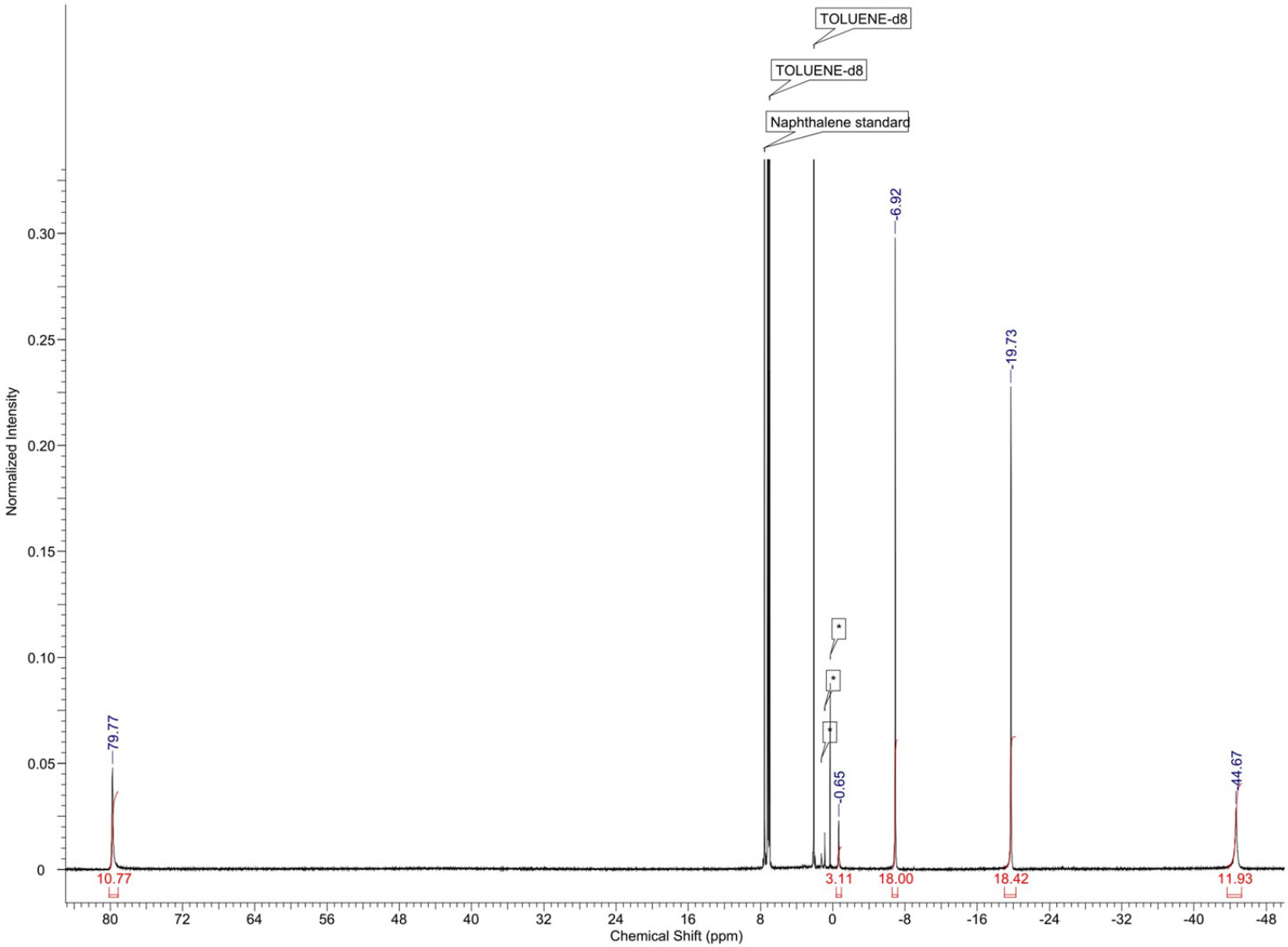


**Figure S1.** $^{1}$H NMR spectrum of $Fe_3H_3$**L** (**1**) in toluene-$d_8$.

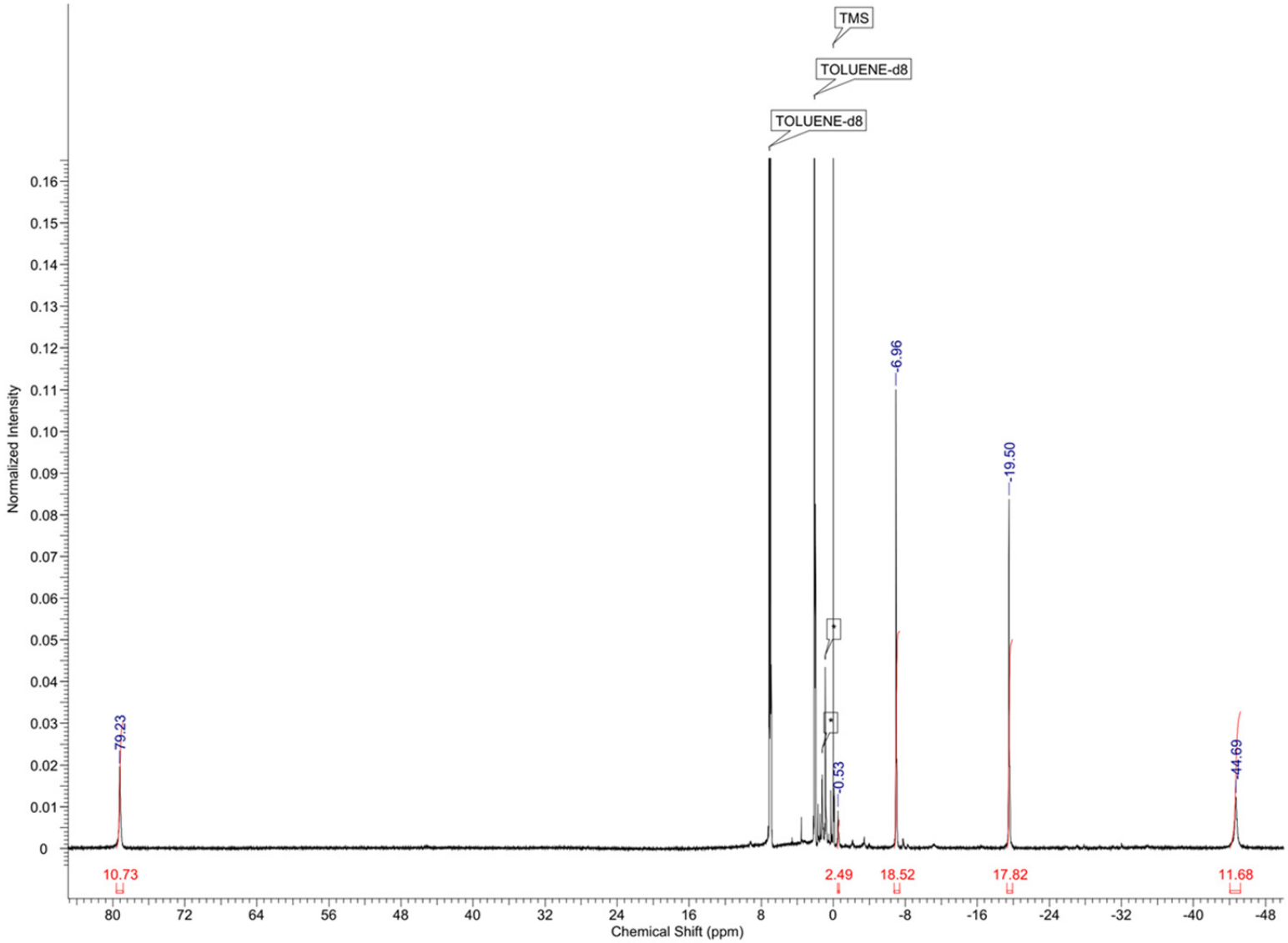


**Figure S2.** $^{1}$H NMR spectrum of $Fe_3D_3$**L** (**1-D$_3$**) in toluene-$d_8$.

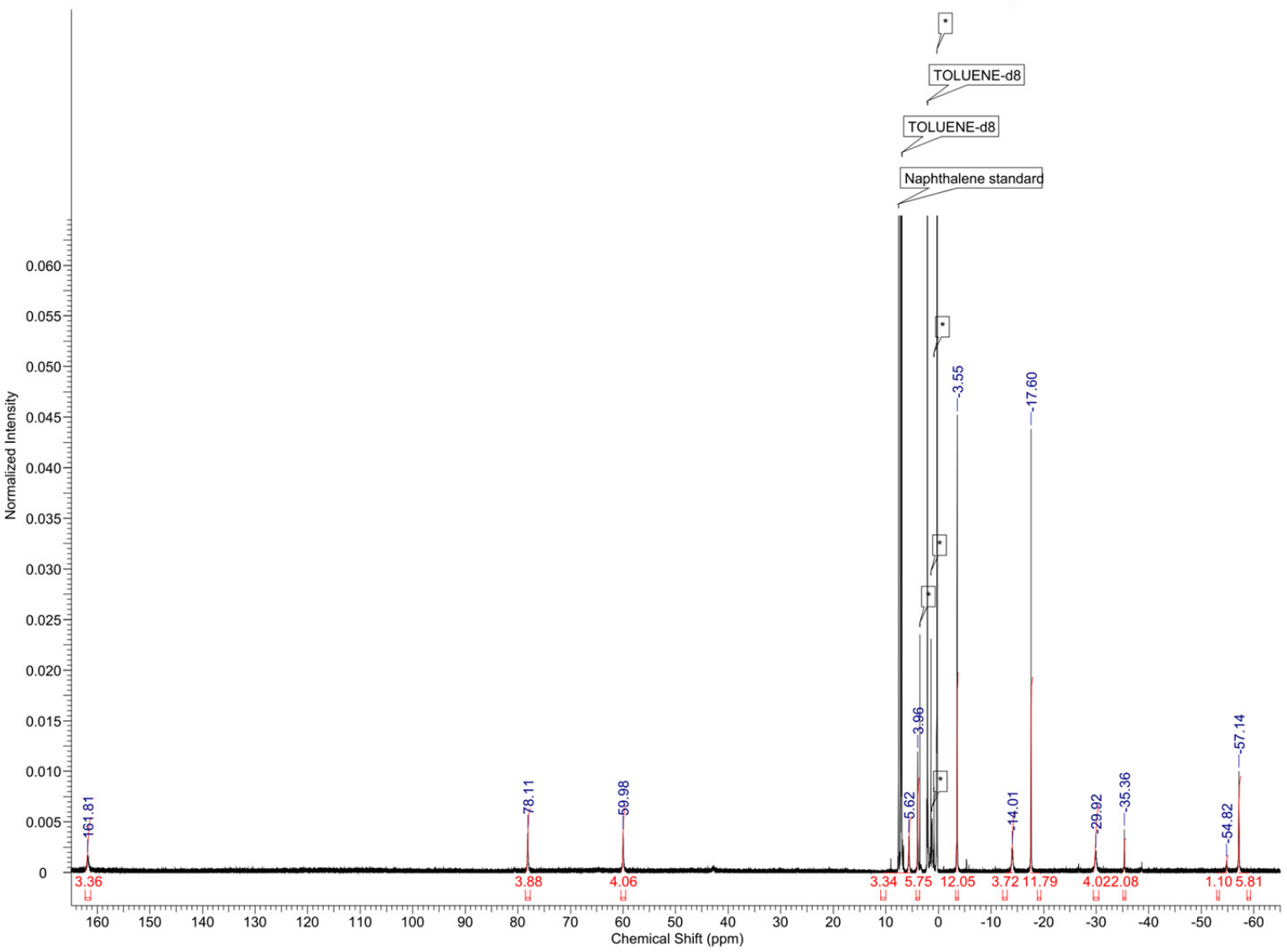


**Figure S3.** $^{1}$H NMR spectrum of $(FeCO)_2Fe(\mu_3\text{-}H)$**L** (**2**) in toluene-$d_8$.

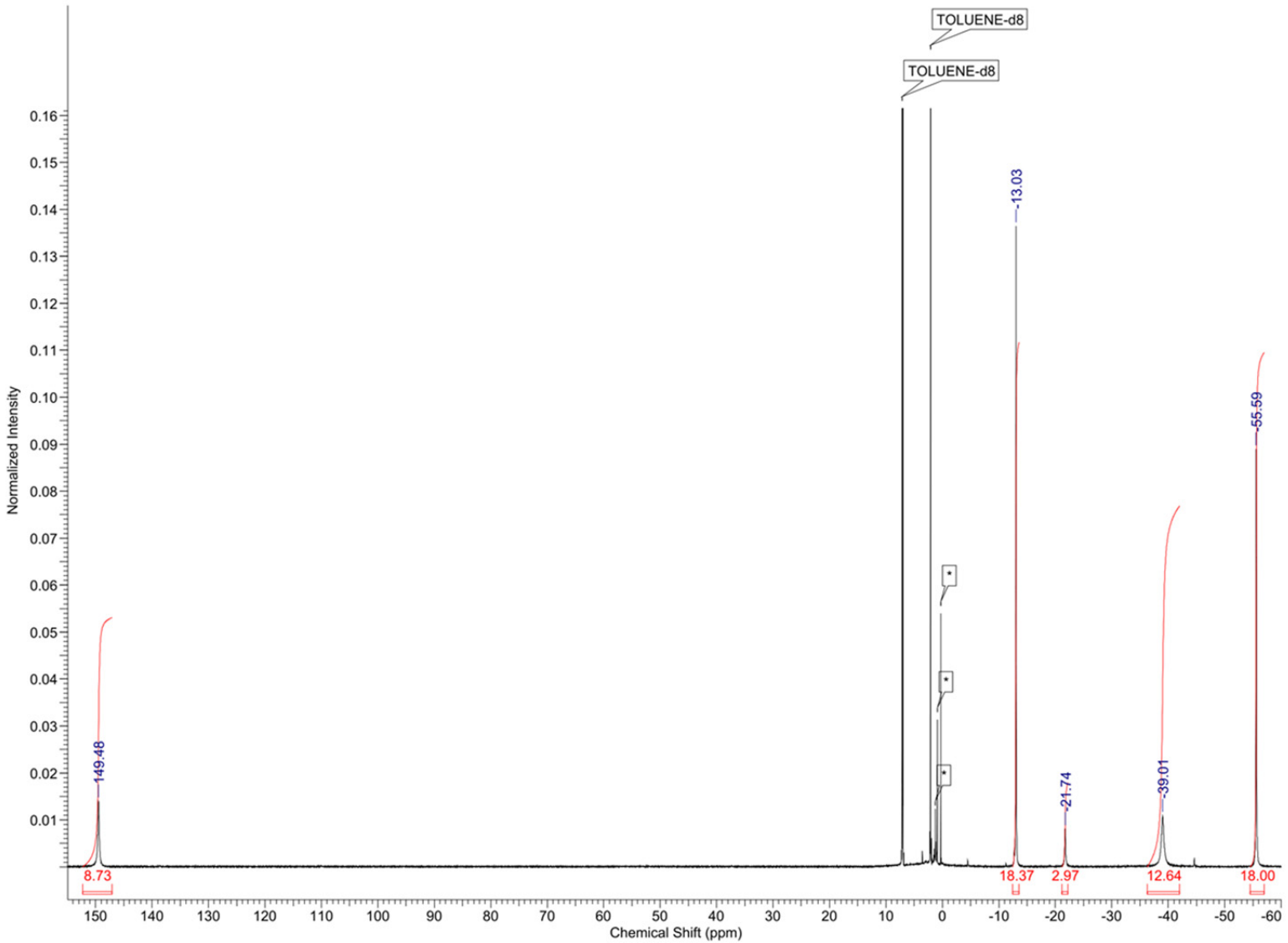


**Figure S4.** $^{1}$H NMR spectrum of $Fe_3F_3$**L** (**3**) in toluene-$d_8$.

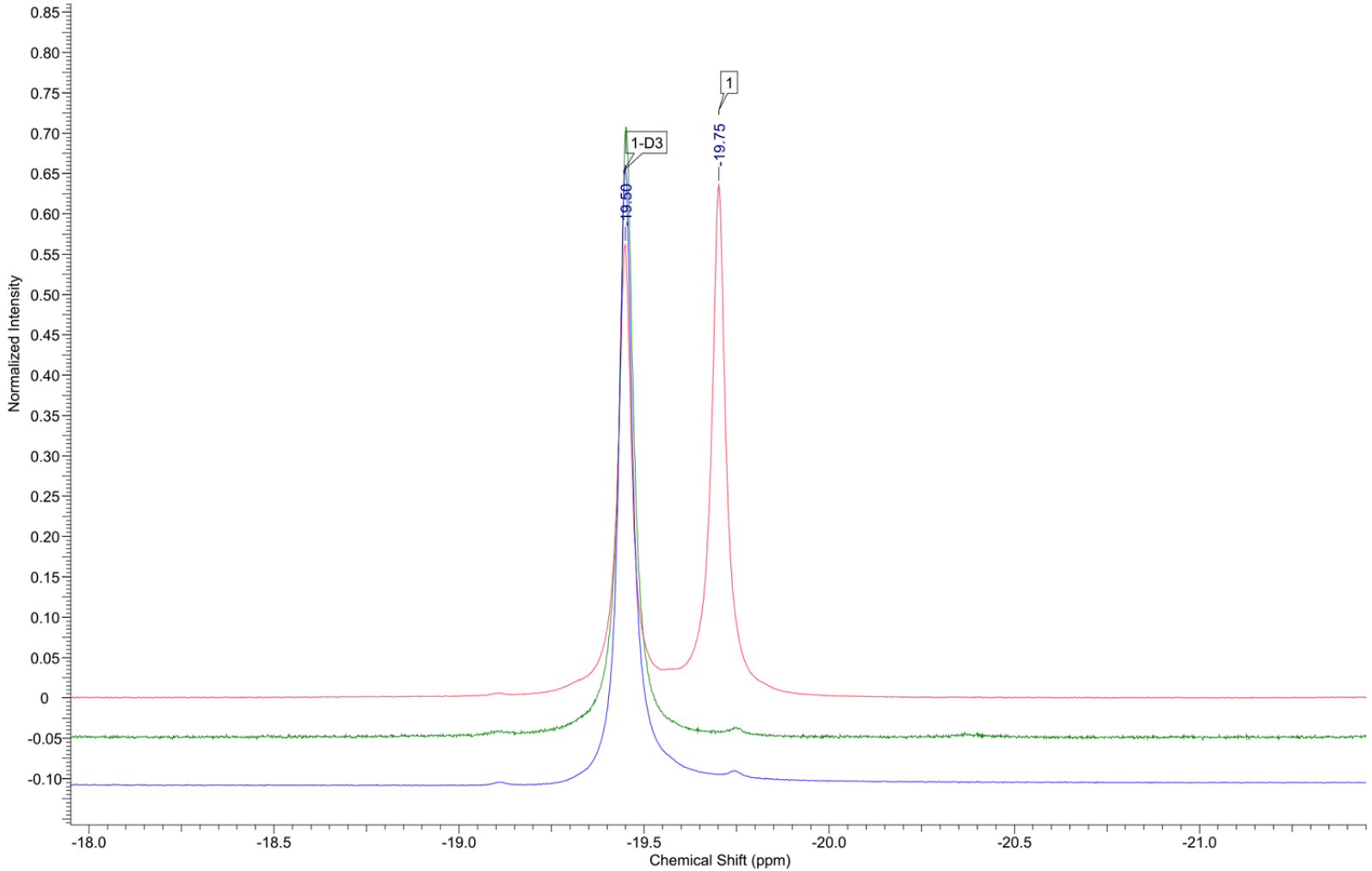


**Figure S5.** $^{1}$H NMR spectra in toluene-$d_8$ of **1-D$_3$** (blue) and a mixture of **1** and **1-D$_3$** (red) compared with the attempted reaction of **1-D$_3$** with $H_2$ (green), indicating that **1** does not form.

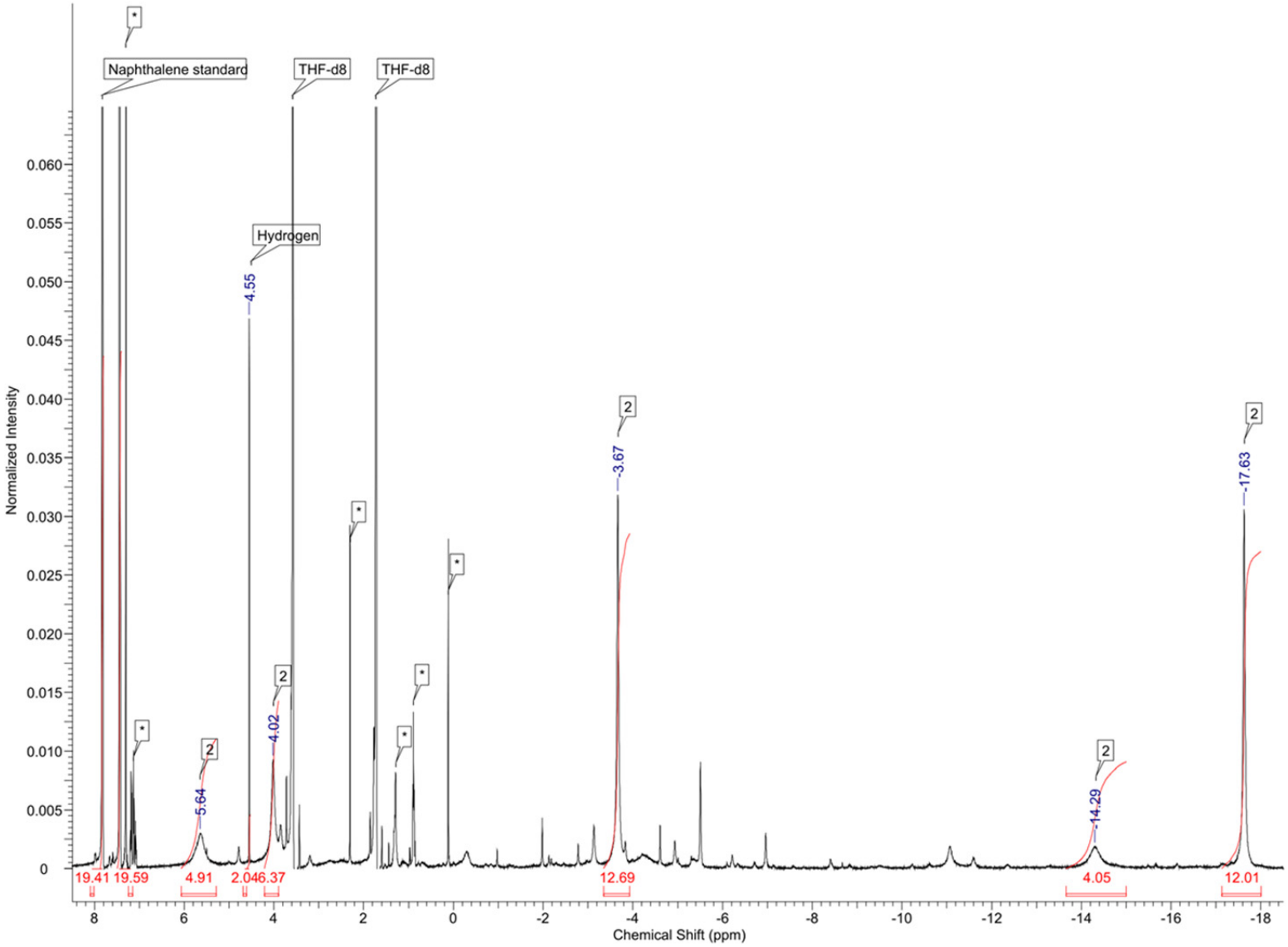


**Figure S6.** A portion of the *in situ* $^{1}$H NMR spectrum in THF-$d_8$ of the reaction of $Fe_3H_3$**L** (**1**) with CO showing the generation of $H_2$.

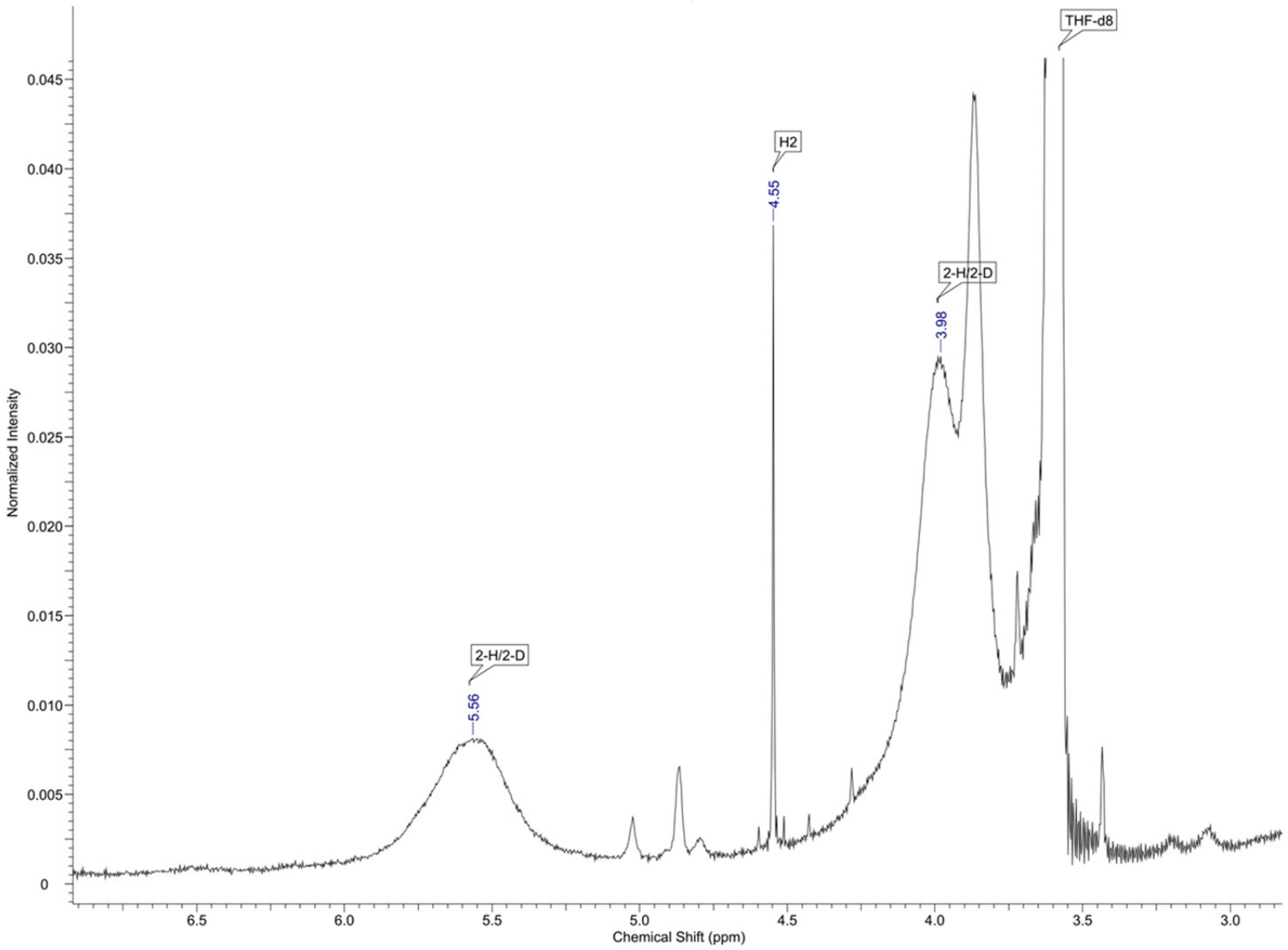


**Figure S7.** A portion of the *in situ* $^{1}$H NMR spectrum in THF-$d_8$ of the reaction of a mixture of $Fe_3H_3$**L** (**1**) and $Fe_3D_3$**L** (**1-D**) with CO showing the generation of $H_2$ but not HD.

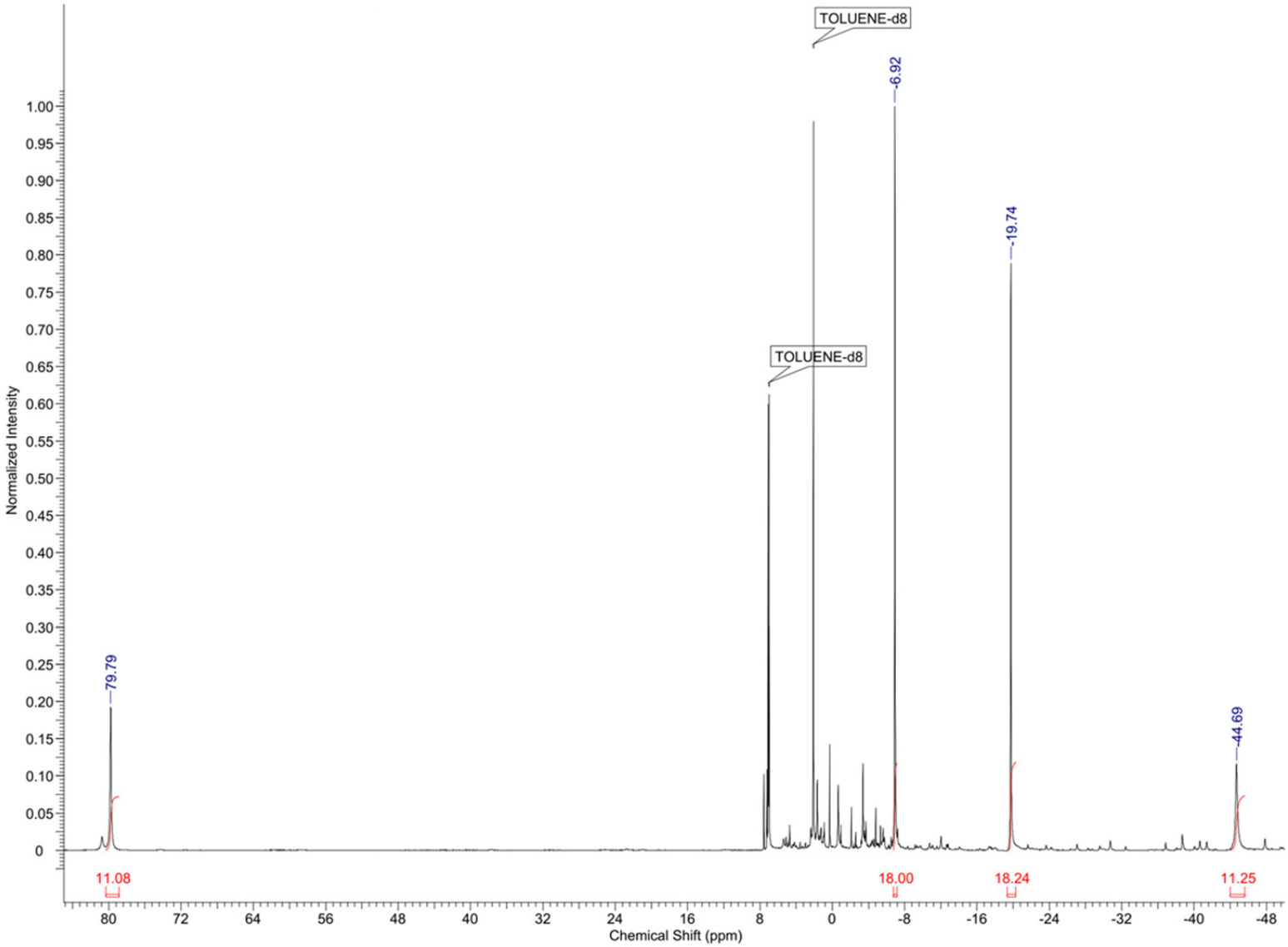


**Figure S8.** $^{1}$H NMR spectrum in toluene-$d_8$ of $Fe_3H_3$**L** (**1**) produced by treatment of **2** with $H_2$.

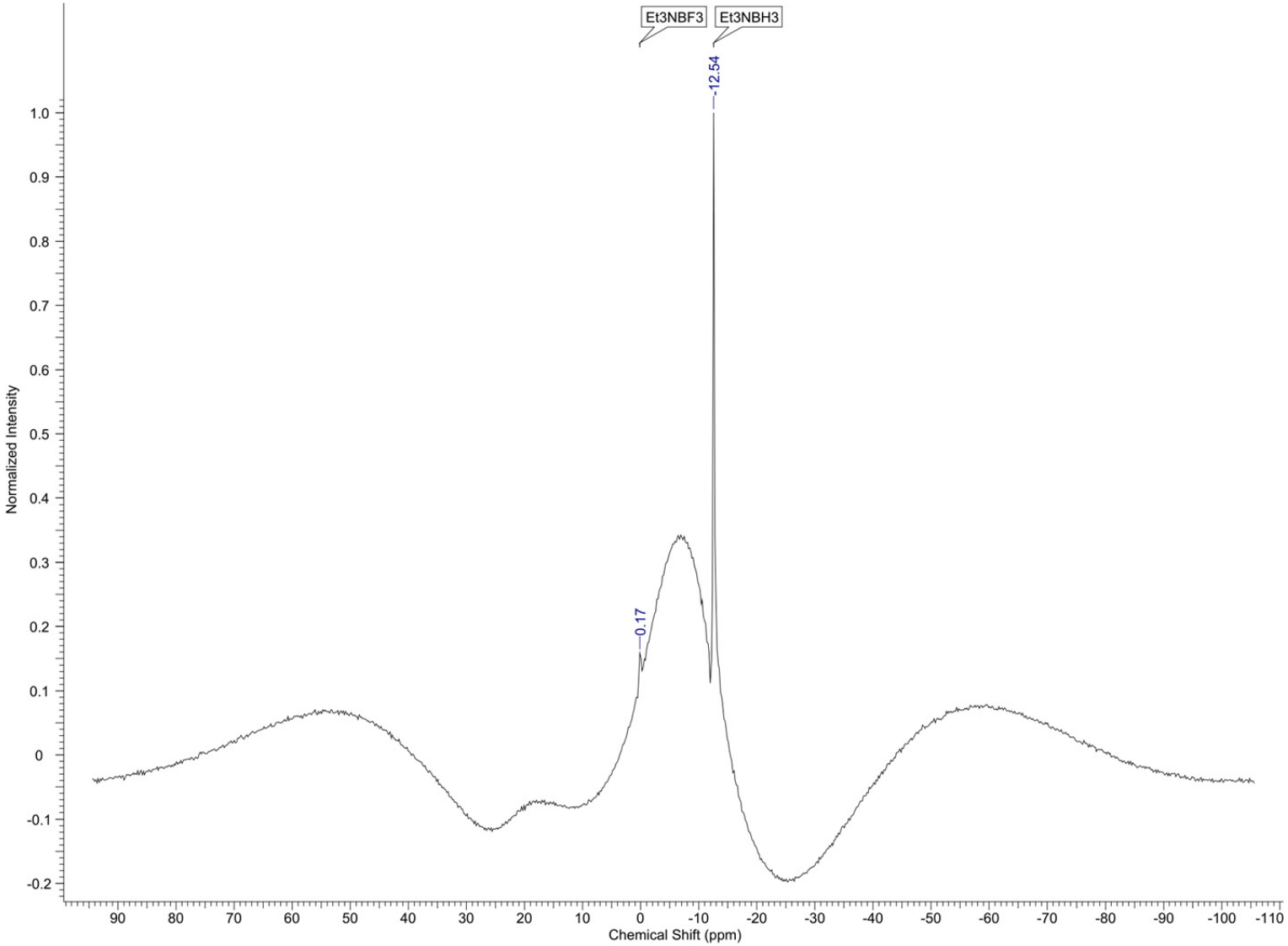


**Figure S9.** $^{11}$B NMR spectrum of the reaction of $Fe_3H_3$**L** (**1**) with $BF_3$•$OEt_2$ after treatment with $NEt_3$.

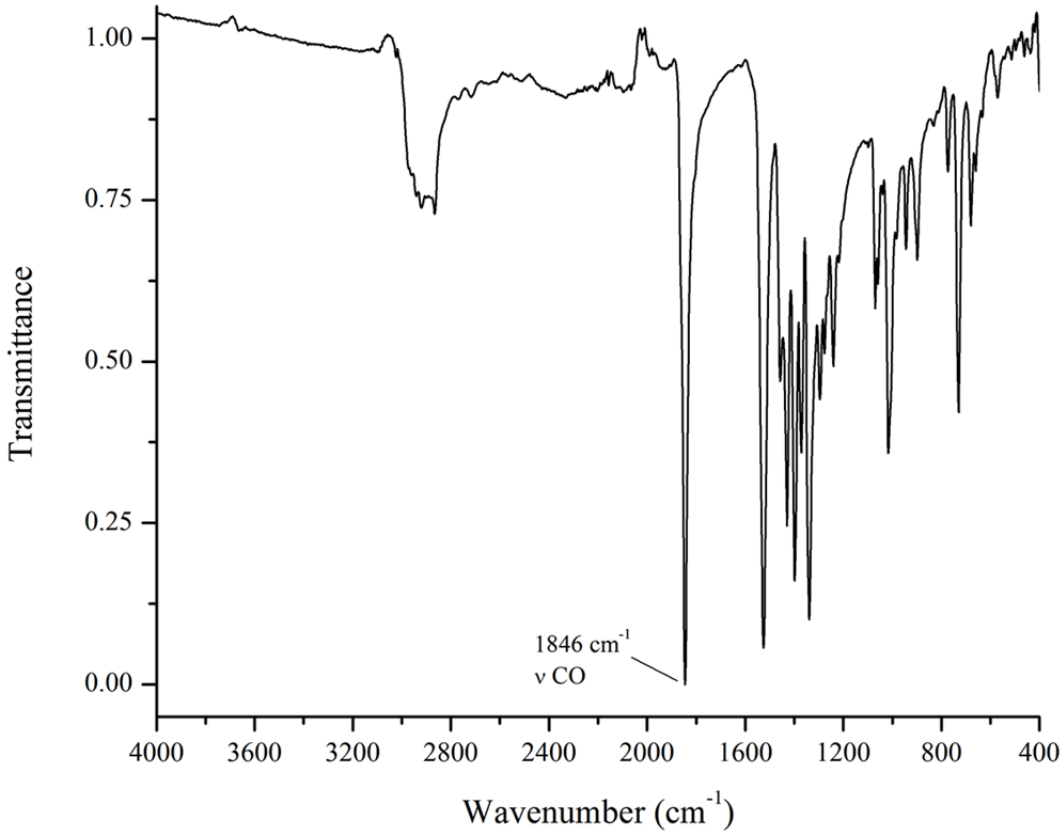


**Figure S10.** IR spectrum of $(FeCO)_2Fe(\mu_3\text{-}H)$**L** (**2**).

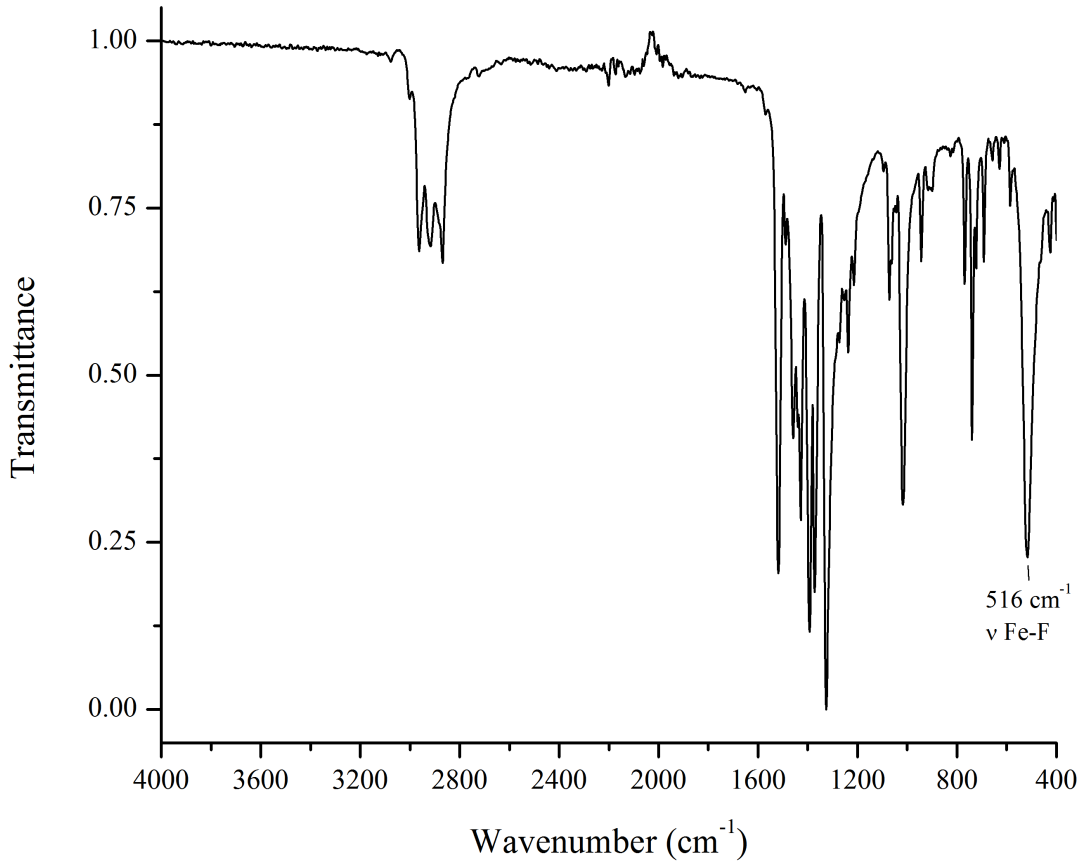


**Figure S11.** IR spectrum of $Fe_3F_3$**L** (**3**).

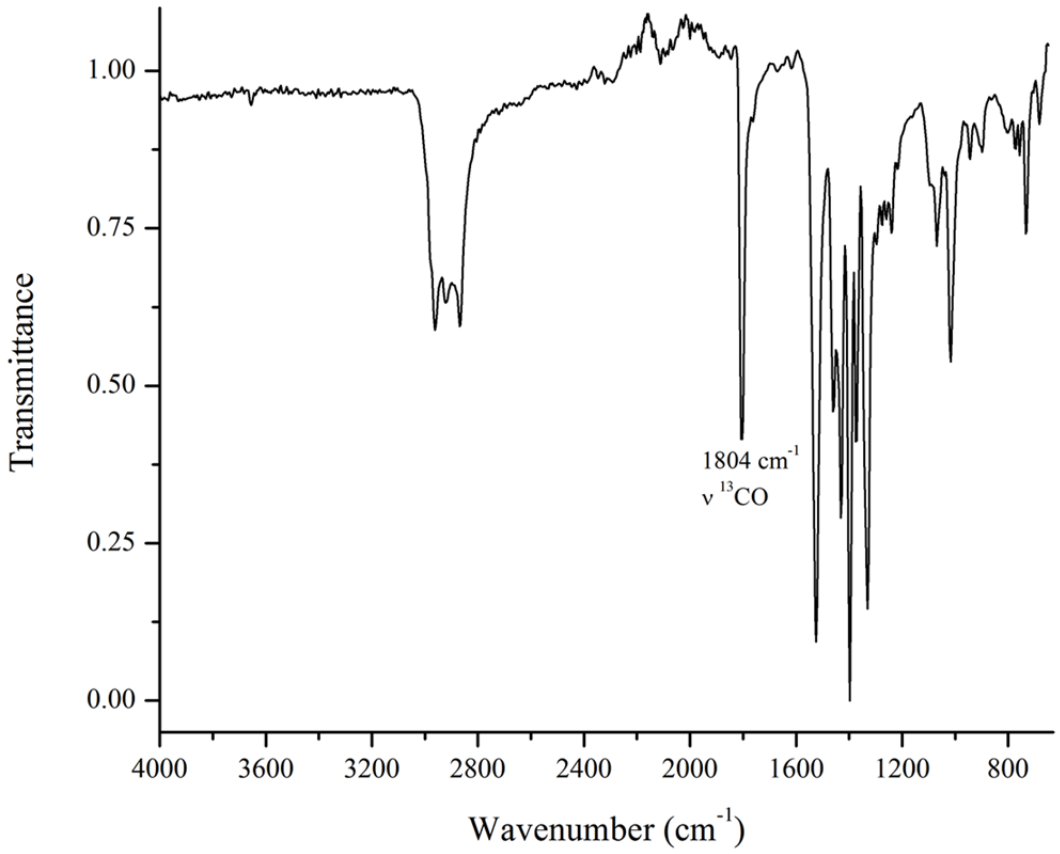


**Figure S12.** IR spectrum of $(Fe^{13}CO)_2(\mu_3\text{-H})$**L** (**2-$^{13}$CO**).

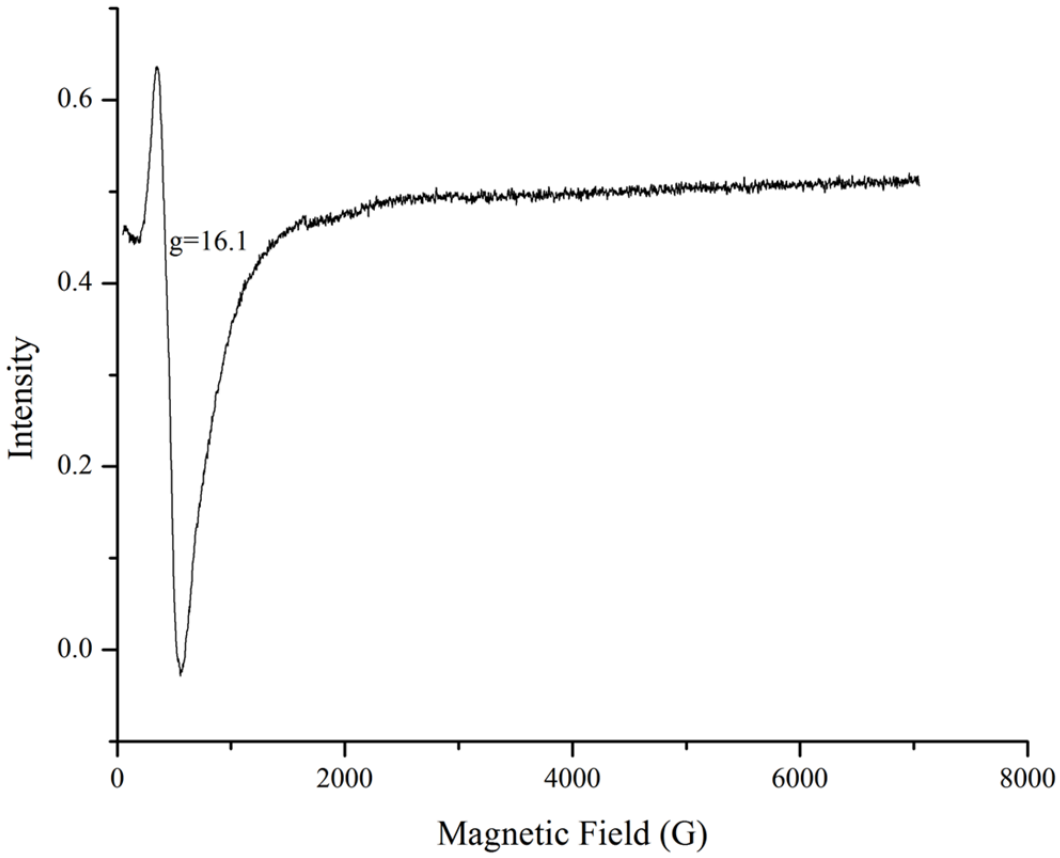


**Figure S13.** Powder X-band EPR spectrum of **2** in parallel mode at 5 K. Acquisition parameters: 3550 ± 3500 G sweep range, 3500 points, 5 G modulation amplitude, 100 kHz modulation frequency, 40ms conversion time, 31dB attenuation.

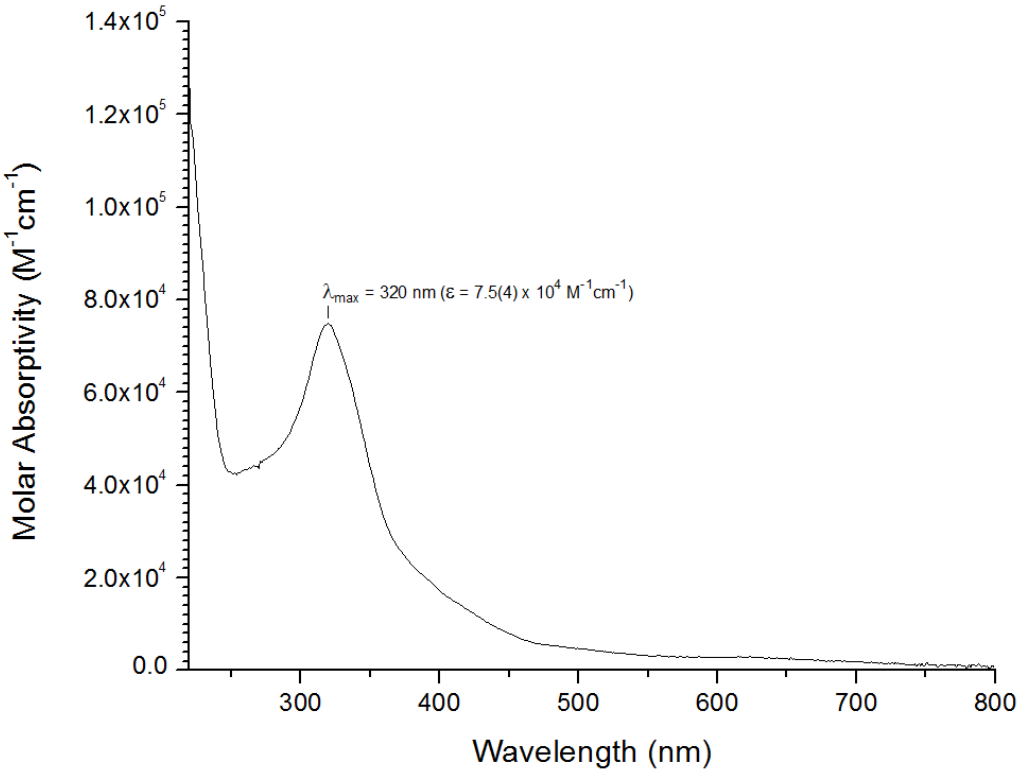


**Figure S14.** UV-vis spectrum of $(FeCO)_2Fe(\mu_3\text{-}H)$**L** (**2**) in THF.

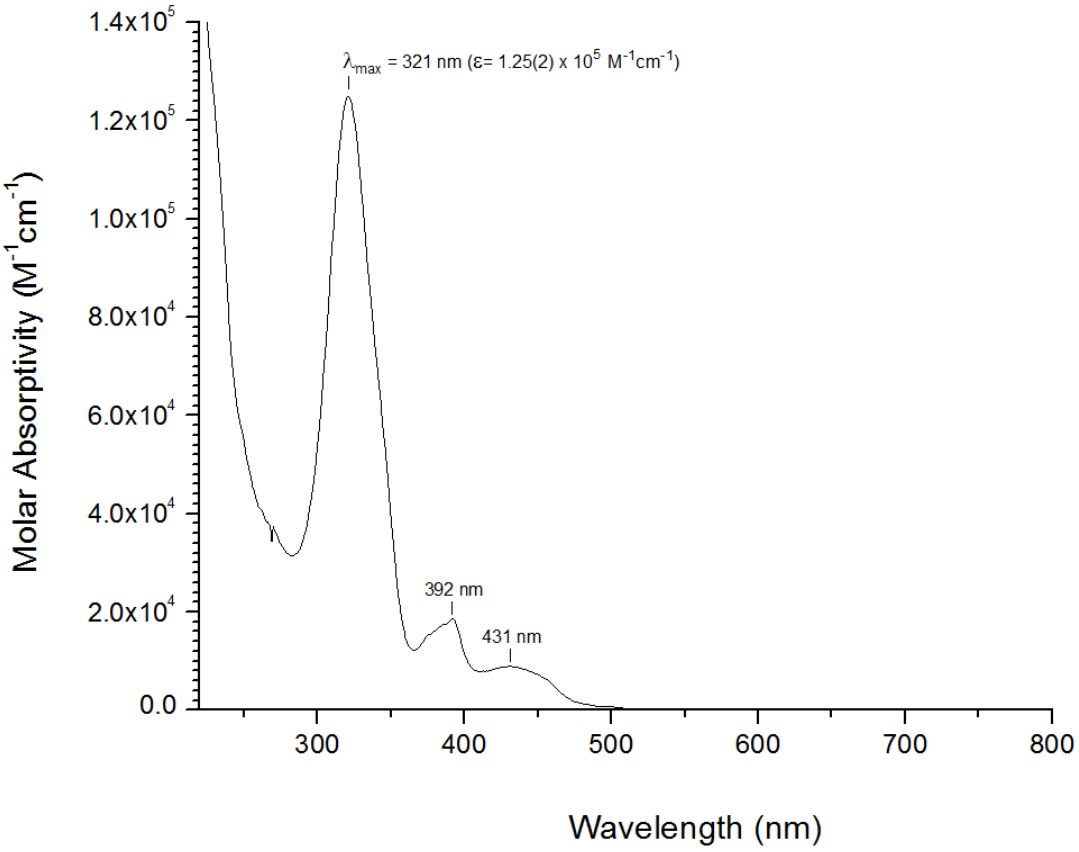


**Figure S15.** UV-vis spectrum of $Fe_3F_3$**L** (**3**) in THF.

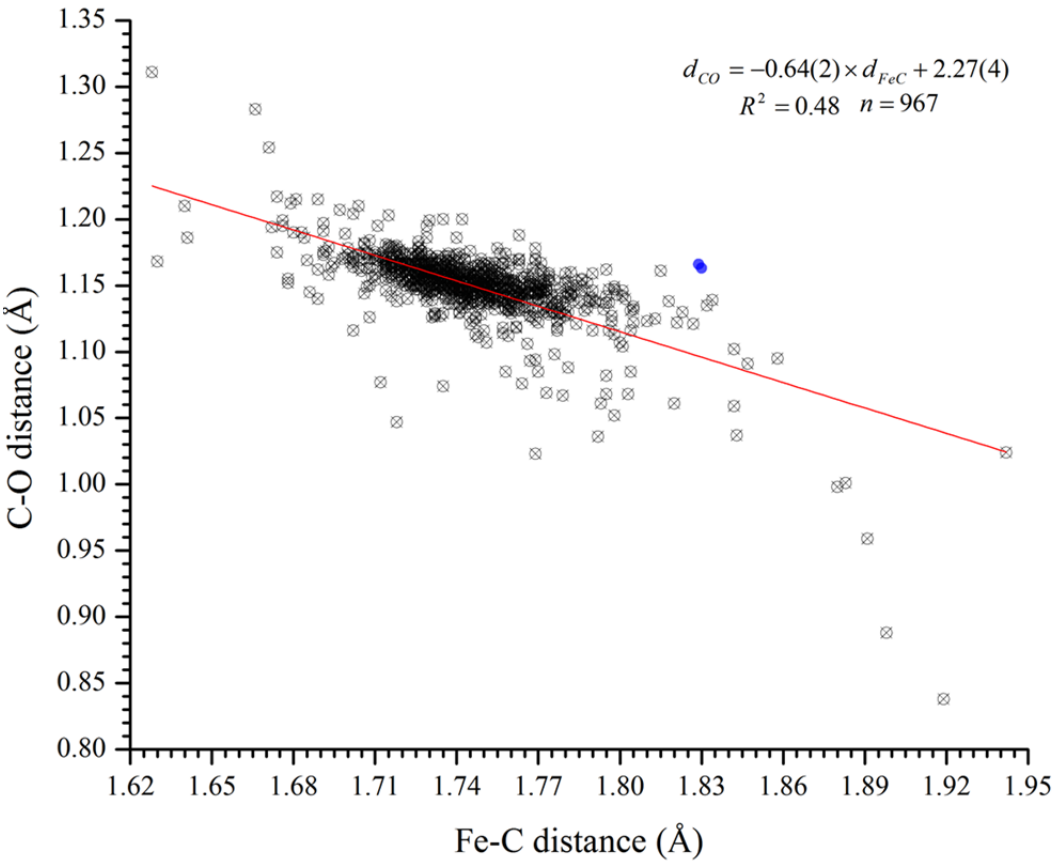


**Figure S16.** Plot of C-O distance versus Fe-C distance for **2** (filled blue circles) compared with complexes in the CSD featuring the monocarbonyliron motif (gray circles with X marks). Search criteria: Fe-C≡O NOT $Fe(CO)_2$ NOT Fe($\mu$-CO)M NOT Fe($\mu$-$\eta^1$:$\eta^1$-CO)M.

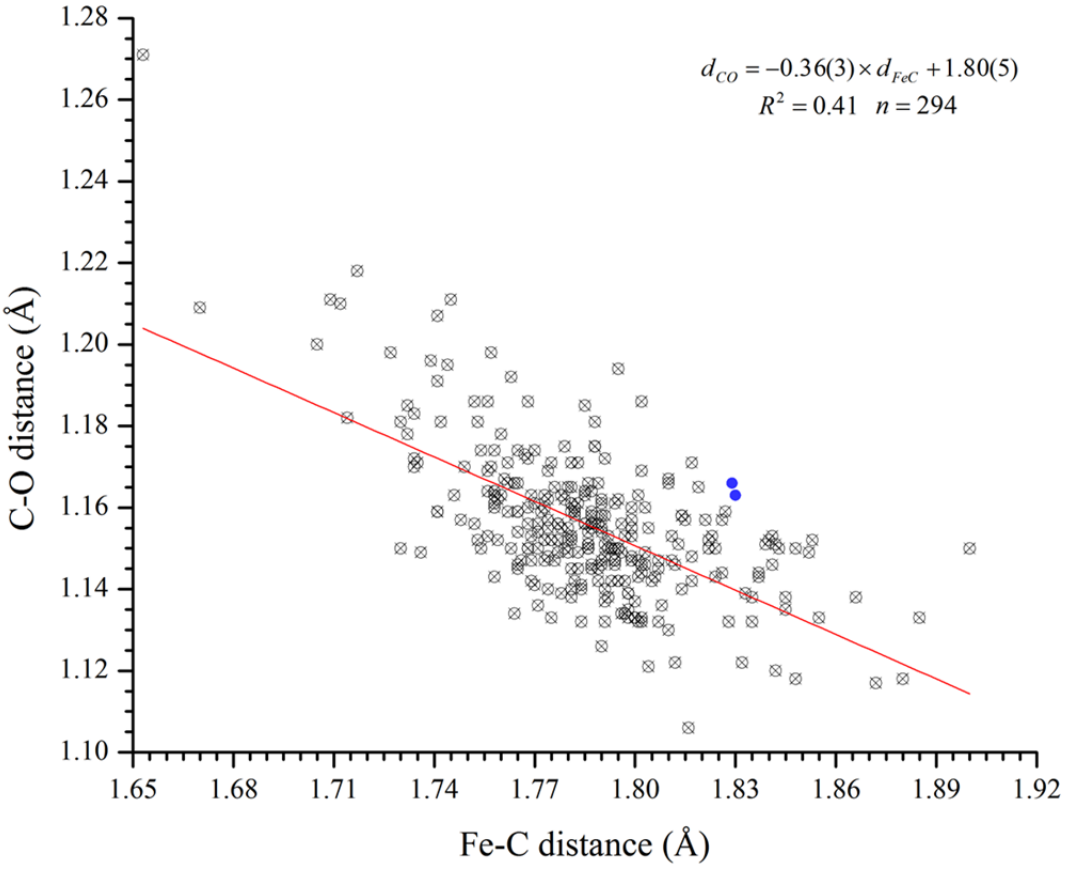


**Figure S17.** Plot of C-O distance versus Fe-C distance for **2** (filled blue circles, $(Fe\cdots CO)_{average}$ = 2.51 Å) compared with iron carbonyl complexes in the CSD featuring Fe···CO semi-bridging interactions similar to those in **2** (gray circles with X marks, Fe···CO range 2.51 ± 0.1 Å). Search criteria: Fe-C≡O AND Fe···C≡O with Fe···C distance 2.51 ± 0.1 Å.

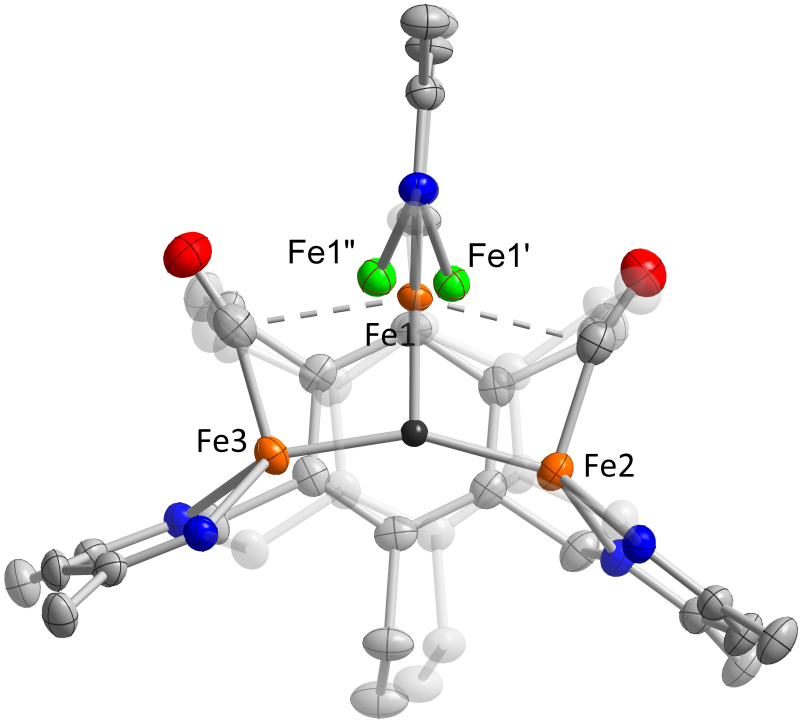


**Figure S18.** Top-down view of the solid state structure of $(FeCO)_2Fe(\mu_3\text{-}H)$**L** (**2**) showing the minor occupied site for Fe1. Fe1' and Fe1" (green spheres) are modeled with occupancies of 3.5% and 2.5%, respectively. C, N, O, amd Fe atoms modeled as gray, blue, red, and orange thermal ellipsoids (75% probability). The brigding hydride is shown as a black sphere. All other H-atoms and solvent molecules are omitted for clarity.

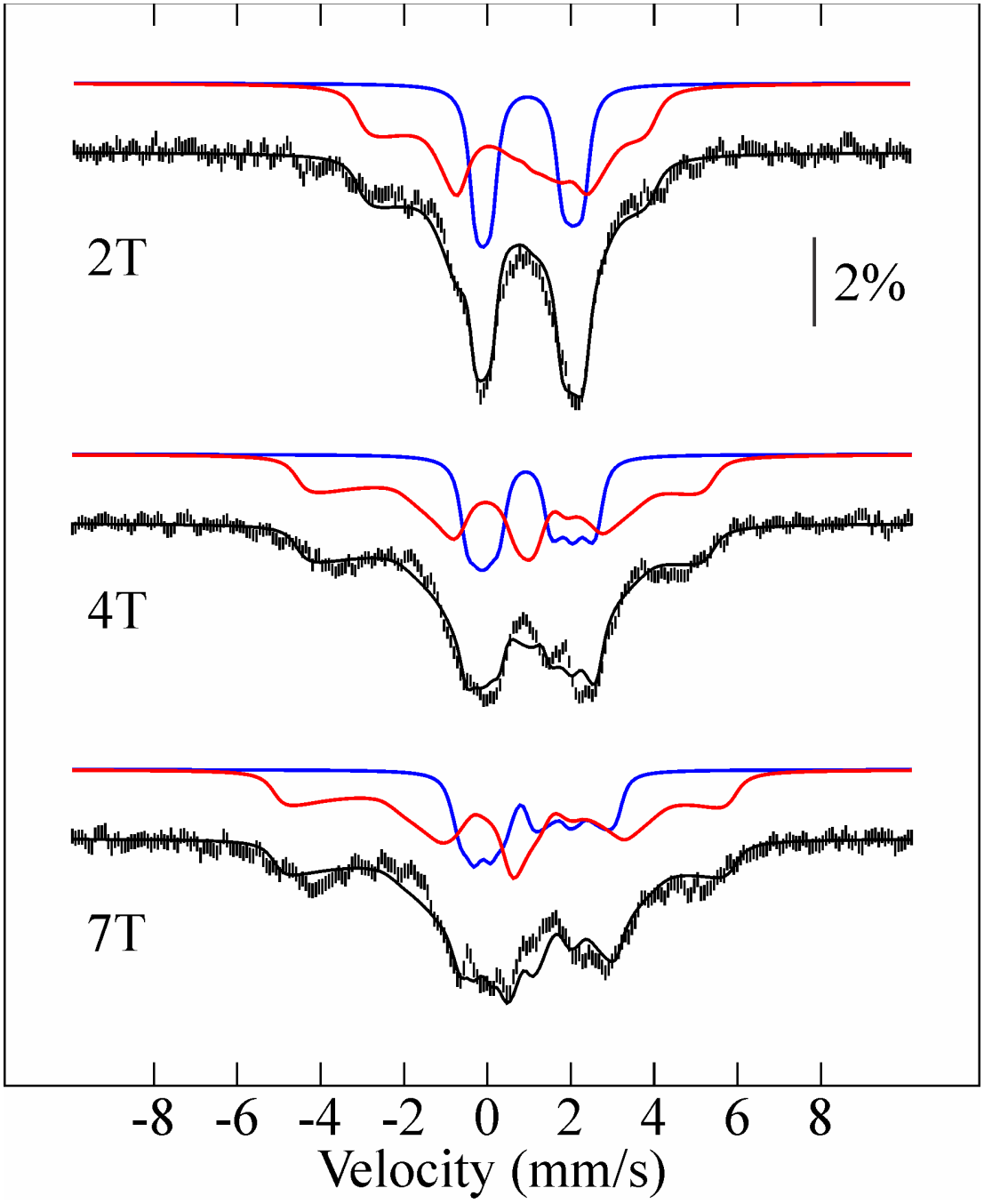


**Figure S19.** 4.8 K Mössbauer spectra of **2** measured in different parallel applied magnetic fields**.** The vertical bars are the experimental points. The blue lines are S = 2 spin-Hamiltonian simulations with D = 15 $cm^{-1}$, E/D = 0, $g_x = g_y = g_z = 2$, $\delta = 0.98$ mm/s, $\Delta E_Q = 2.14$ mm/s, $\eta = 0.97$, **A** = (-4, 3, -32) T, and account for 1/3 of total iron. The red lines are S = 3/2 spin-Hamiltonian simulations with D = 2 $cm^{-1}$, E/D = 0.15, $g_x = g_y = g_z = 2$, $\delta = 0.66$ mm/s, $\Delta E_Q = 2.58$ mm/s, $\eta = 0.54$, **A** = (-28, -3, 13) T, and account for 2/3 of total iron. The black lines overlaid with the experimental data are the composite theoretical spectra.

**Table S1.** Simulation parameters for the quadrupole doublets in the Mössbauer spectrum of **2** measured under zero applied field at 80 K.

| doublet | $\delta$ (mm/s) | $\Delta E_Q$ (mm/s) | $\Gamma$ (mm/s) | % |
|---|---|---|---|---|
| a (blue) | 0.98 | 2.15 | 0.27 | 1/3 |
| b (red) | 0.66 | 2.60 | 0.31 | 2/3 |

**Table S2.** Selected bond distances and angles of the crystal structures of **1** and **3** compared with other iron *β*-diketiminates ($N_L$ = nacnac N-donor atom, X = H, O, N, F, or S, bite angle = $N_L$–Fe–$N_L$).

| Complex | Fe–$N_L$ (Å) | Fe–X (Å) | Bite angle (°) |
|---|---|---|---|
| 1[2] | 2.039(2)–2.057(2) | 1.78(3)–1.86(3) | 90.23(8)–91.10(8) |
| S1[6] | 2.043(2)–2.046(2) | 1.963(3)–1.978(2) | 96.84(9)–97.1(1) |
| 3 | 1.984(4)–1.990(4) | 1.943(3)–1.967(3) | 96.6(2)–96.8(2) |
| S2[6] | 2.029(3)–2.044(3) | 1.958(3)–1.975(3) | 94.9(1)–95.1(1) |
| S3[7] | 2.003(2) | 2.1827(8)–2.1911(8) | 99.0(1) |
| S4[8] | 2.008(2)–2.016(2) | 1.976(1)–1.977(1) | 93.27(7) |
| S5[8] | 1.961(1) | 1.808(2) | 95.66(8) |
| S6[9] | 2.037(1)–2.042(1) | 2.029(4)–2.082(4) | 92.39(5) |

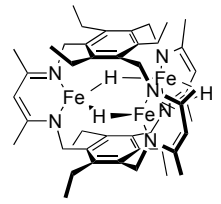


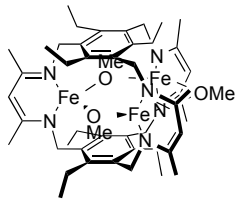


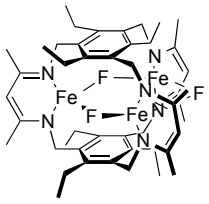


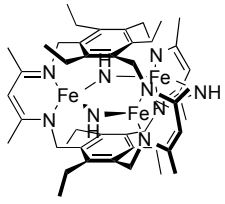


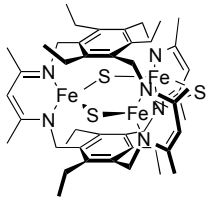


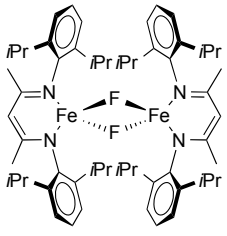


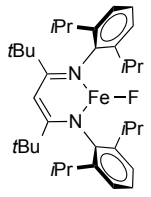


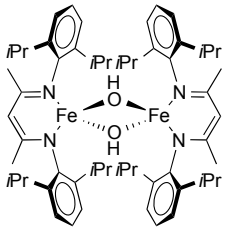

**Table S3.** Crystal data and structure refinement for $(FeCO)_2Fe(\mu_3\text{-}H)$**L** (**2**).

| | | |
|---|---|---|
| Identification code | kand16 | |
| Empirical formula | C59 H76 Fe3 N6 O2 | |
| Formula weight | 1068.80 | |
| Temperature | 100(2) K | |
| Wavelength | 0.71073 Å | |
| Crystal system | Triclinic | |
| Space group | Pī | |
| Unit cell dimensions | a = 12.5204(6) Å | α= 77.1659(11)°. |
| | b = 13.0808(7) Å | β= 87.1605(10)°. |
| | c = 16.5376(8) Å | γ = 84.1531(11)°. |
| Volume | 2626.1(2) $Å^3$ | |
| Z | 2 | |
| Density (calculated) | 1.352 $Mg/m^3$ | |
| Absorption coefficient | 0.867 $mm^{-1}$ | |
| F(000) | 1132 | |
| Crystal size | 0.275 x 0.098 x 0.086 $mm^3$ | |
| Theta range for data collection | 1.263 to 27.500°. | |
| Index ranges | -16≤h≤16, -16≤k≤16, -21≤l≤21 | |
| Reflections collected | 50075 | |
| Independent reflections | 12038 [R(int) = 0.0290] | |
| Completeness to theta = 25.242° | 100.0 % | |
| Absorption correction | Analytical | |
| Max. and min. transmission | 0.9426 and 0.8105 | |
| Refinement method | Full-matrix least-squares on $F^2$ | |
| Data / restraints / parameters | 12038 / 0 / 655 | |
| Goodness-of-fit on $F^2$ | 1.085 | |
| Final R indices [I>2sigma(I)] | R1 = 0.0304, wR2 = 0.0820 [9908] | |
| R indices (all data) | R1 = 0.0404, wR2 = 0.0882 | |
| Extinction coefficient | n/a | |
| Largest diff. peak and hole | 0.603 and -0.489 $e.Å^{-3}$ | |

$R1 = \Sigma(||F_o| - |F_c||) / \Sigma|F_o|$

$wR2 = [\Sigma[w(F_o^2 - F_c^2)^2] / \Sigma[w(F_o^2)^2]]^{1/2}$

$S = [\Sigma[w(F_o^2 - F_c^2)^2] / (n-p)]^{1/2}$

$w= 1/[\sigma^2(F_o^2)+(m*p)^2+n*p]$, $p = [\max(F_o^2,0)+ 2* F_c^2]/3$, m & n are constants.

**Table S4**. Crystal data and structure refinement for $Fe_3F_3$**L** (**3**).

| | | |
|---|---|---|
| Identification code | murray08_sq | |
| Empirical formula | C45 H63 F3 Fe3 N6 | |
| Formula weight | 912.50 | |
| Temperature | 100 K | |
| Wavelength | 0.71073 Å | |
| Crystal system | Monoclinic | |
| Space group | Cc | |
| Unit cell dimensions | a = 20.7273(14) Å | α = 90°. |
| | b = 11.4948(8) Å | β = 112.429(3)°. |
| | c = 21.957(2) Å | γ = 90°. |
| Volume | 4835.7(7) $Å^3$ | |
| Z | 4 | |
| Density (calculated) | 1.273 $Mg/m^3$ | |
| Absorption coefficient | 0.936 $mm^{-1}$ | |
| F(000) | 1948 | |
| Crystal size | 0.29 x 0.27 x 0.24 $mm^3$ | |
| Theta range for data collection | 2.583 to 26.390°. | |
| Index ranges | -25<=h<=25, -12<=k<=14, -23<=l<=27 | |
| Reflections collected | 16564 | |
| Independent reflections | 7136 [R(int) = 0.0399] | |
| Completeness to theta = 25.000° | 99.7 % | |
| Absorption correction | Semi-empirical from equivalents | |
| Max. and min. transmission | 0.2602 and 0.2152 | |
| Refinement method | Full-matrix least-squares on $F^2$ | |
| Data / restraints / parameters | 7136 / 2 / 526 | |
| Goodness-of-fit on $F^2$ | 1.012 | |
| Final R indices [I>2sigma(I)] | R1 = 0.0356, wR2 = 0.0899 | |
| R indices (all data) | R1 = 0.0421, wR2 = 0.0932 | |
| Absolute structure parameter | 0.028(10) | |
| Extinction coefficient | n/a | |
| Largest diff. peak and hole | 0.400 and -0.277 $e.Å^{-3}$ | |
| SQUEEZE | 108e/uc | |

**References.**


1. (a) Evans, D. F. *J. Chem. Soc.* **1959**, 2003-2005. (b) Bain, G. A.; Berry, J. F. *J. Chem. Educ.* **2008**, *85*, 532-536. (c) Sur, S. K. *J. Magn. Reson.* **1989**, *82*, 169-173. (d) Schubert, E. M. *J. Chem. Educ.* **1992**, *69*, 62.
2. Lee, Y.; Anderton, K. J.; Sloane, F. T.; Ermert, D. M.; Abboud, K. A.; García-Serres, R.; Murray, L. J. *J. Am. Chem. Soc.* **2015**, *137*, 10610-10617.
3. Brown, H.C.; Khuri, A.; Kim, S.C. *Inorg. Chem.* **1977**, *16*, 2229-2233.
4. *SHELXTL2014* (2014). Bruker-AXS, Madison, Wisconsin, USA.
5. G. M. Sheldrick, *SHELXTL-Plus Structure Determination Software Programs* (2014).
6. Lee, Y.; Sloane, F. T.; Blondin, G.; Abboud, K. A.; García-Serres, R.; Murray, L. J. *Angew. Chem. Int. Ed.* **2015**, *54*, 1499-1503.
7. Lee, Y.; Jeon, I.-R.; Abboud, K. A.; García-Serres, R.; Shearer, J.; Murray, L. J. *Chem. Commun.* **2016**, *52*, 1174-1177.
8. Vela, J.; Smith, J. M.; Yu, Y.; Ketterer, N. A.; Flaschenriem, C. J.; Lachicotte, R. J.; Holland, P. L. *J. Am. Chem. Soc.* **2005**, *127*, 7857-7870.
9. Yu, Y.; Sadique, A. R.; Smith, J. M.; Dugan, T. R.; Cowley, R. E.; Brennessel, W. W.; Flaschenriem, C. J.; Bill, E.; Cundari, T.; Holland, P. *J. Am. Chem. Soc.* **2008**, *130*, 6624-6638.